Received 30 September 2021; accepted 2 November 2021. Date of publication 10 November 2021; date of current version 22 November 2021.
The review of this article was arranged by Editor Z. Zhang.

Digital Object Identifier 10.1109/JEDS.2021.3127013

Quenching Statistics of Silicon Single Photon Avalanche Diodes

THIBAULD CAZIMAJOU [1], MARCO PALA [1] (Member, IEEE), JÉRÔME SAINT-MARTIN [1], RÉMI HELLEBOID [2], JÉRÉMY GREBOT [2], DENIS RIDEAU [2], AND PHILIPPE DOLLFUS [1] (Member, IEEE)

1 Université Paris–Saclay, CNRS, Centre de Nanosciences et de Nanotechnologies, 91120 Palaiseau, France
2 STMicroelectronics, DPOSIM, 38920 Crolles, France

CORRESPONDING AUTHOR: T. CAZIMAJOU (e-mail: thibauld.cazimajou@universite-paris-saclay.fr)

This work was supported in part by the French Industry Ministry (Nano2022 Project under IPCEI Program) and in part by the French ANR through the Project GeSPAD under Grant ANR-20-CE24-0004.

This article has supplementary downloadable material available at https://doi.org/10.1109/JEDS.2021.3127013, provided by the authors.

ABSTRACT The statistical behavior of silicon-based single-photon-avalanche-diodes (SPADs) is investigated by using self-consistent 3-D Monte Carlo simulations. The coupling of Poisson and Boltzmann transport equations allows us to go beyond the analysis of avalanche breakdown and its timing and to extend the investigation to the quenching of the photodetector circuit. We find out that the quenching of SPADs is probabilistic and strongly depends on the surrounding circuit, in particular on the so-called quenching resistance. Independently of the SPAD deadtime, it appears that the extinction time needed to suppress any avalanche event may vary over a very large range.

INDEX TERMS Avalanche breakdown, Monte Carlo methods, avalanche photodiodes.

I. INTRODUCTION

Single Photon Avalanche Diodes are fast and sensible photodetectors that can be used for a wide range of applications, including quantum computing [1], quantum cryptography [2], 3D laser detection [3] and imaging, fluorescence lifetime imaging [4]. A SPAD is essentially a reverse biased p-n or p-i-n junction, with an applied voltage V_D higher than the breakdown voltage V_B. Under such conditions, an electron-hole (e-h) pair generated by photon absorption can be accelerated by the electric field, triggering impact ionization and the generation of new e-h pairs. This avalanche phenomenon leads to a strong increase of the diode current, which makes possible the detection of photon absorption at the circuit level.

By using particle Monte Carlo (MC) method for solving the Boltzmann transport equation (BTE), different aspects of SPAD operation have been studied using either simplified [5], [6] or full-band MC approach [7]. These works have allowed the detailed statistical analysis of avalanche breakdown probability, excess noise factor, time to avalanche (delay between photon absorption and onset of measurable current), jitter (due to statistical spreading of transit times and avalanche build up) [7].

Another important stage of operation is the quenching of SPAD, needed to detect a new photon. It is possible to design a passive quenching circuit with a simple RC circuit connected in series with the SPAD [8]. To accurately describe this quenching stage within numerical simulation, it is obviously necessary to consider the self-consistent time evolution of current, bias voltage, carrier density and electric field. To the best of our knowledge, the full SPAD operation in the presence of quenching circuit has mainly been discussed so far on the basis of compact modeling [9] in which the quench is considered as successful if the current becomes smaller than a threshold current [10]. Computationally efficient Verilog-A model and TCAD mixed-mode simulation can be used too [11]. However, these approaches suffer from strong approximations and require extensive calibration. In this paper we go further to consider the intrinsic stochasticity of quenching that has received low attention in the literature [10], [12] and has never been addressed by means of self-consistent MC simulation within the mixed-mode approach. At the cost of high computational time, this approach includes all stochastic features of carrier transport, allowing us to investigate the statistical aspects of SPAD quenching, like

the quenching probability and the distribution of quench duration.

In this letter, a typical silicon SPAD including passive quenching circuit is investigated on the basis of 3-D particle MC simulation self-consistently coupled to the Poisson's equation.

II. MODEL AND SIMULATED DEVICE

The simulated device consists in a silicon PN junction with length $L = 1300$ nm and square cross section of width $W = 300$ nm. The device is connected in series with a passive quenching circuit, here a RC circuit. The diode has a realistic doping profile with doping concentration of 6×10^{17} cm^{-3} and 6.35×10^{17} cm^{-3} for the P- and N-type region, respectively, with a quasi-linear transition region of about 900 nm long. A voltage V_{bias} is applied between the terminals of the circuit composed by the SPAD and quenching circuit in series.

The 3-D particle Monte Carlo code used here has been developed to investigate a large range of devices, including the effect of random distribution of discrete doping impurities [13]. To demonstrate the stochastic aspects of quenching, analytic bands have been considered here. Full band simulations could be used to improve the physical description of hot carrier effects. In this model the conduction band is made of six Δ valleys [14] and four L valleys while the heavy and light hole bands are spherical and non-parabolic, with room-temperature effective masses determined in [15] (see supplementary materials for more details on band structure and scattering parameters). For the SPAD investigation, it is of prime importance to implement a correct description of impact ionization processes for both electrons and holes. For the band structure used here, we implemented Keldysh-like formulations of ionization rates [16] with parameters adjusted, including the power exponent [17], to fit well the experimental field dependence of ionization coefficients [18], [19]. The impact ionization rates implemented here are:

$$\frac{1}{\tau_{ii}}\left[s^{-1}\right] = 1.2\times10^{13}\left(\frac{E-E_G}{E_G}\right)^{2.5} \quad (1)$$

$$\frac{1}{\tau_{ii}}\left[s^{-1}\right] = 1.0\times10^{9}\left(\frac{E-E_G}{E_G}\right)^{2.5} + 2.8\times10^{13}\left(\frac{E-2E_G}{2E_G}\right)^{2} \quad (2)$$

for electrons and holes, respectively, where $E_G = 1.12$ eV is the bandgap in Si. The resulting ionization coefficients are in good agreement with experimental data, as shown in Fig. 1.

For the device simulation, the MC algorithm is coupled with a finite-element Poisson solver. The connection of the SPAD with the passive (R_Q, C_Q) quenching circuit is made in a mixed-mode approach, as follows. At time step $i+1$ the voltage V_D^{i+1} is updated with respect to V_D^i according to

$$V_D^{i+1} = V_D^i + \frac{\Delta t}{R_Q C_Q}\left[-R_Q I^i + \left(V_{bias} - V_D^i\right)\right] \quad (3)$$

where I^i, the current in the device at time step i, is calculated with the Ramo-Shockley theorem [20]. The initial single photon absorption is simulated by generating the first electron-hole (e-h) pair with energy and momentum randomly selected assuming thermal equilibrium distribution.

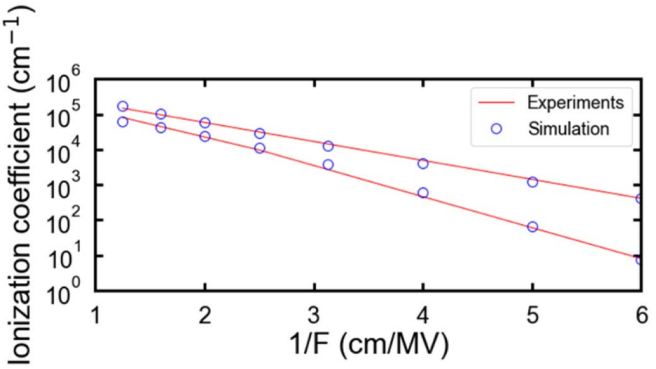

FIGURE 1. Ionization coefficient in Si as a function of inverse electric field. Comparison between experimental data [18], [19] and simulation.

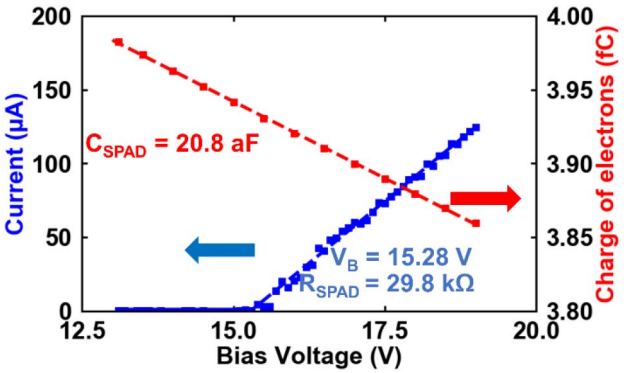

FIGURE 2. Avalanche current (blue squares) and Charge of electrons (red squares) inside the SPAD in steady state function of Bias Voltage. Blue lines and red lines are the linear model used to extract equivalent electric parameters (breakdown voltage V_B, equivalent SPAD resistance R_{SPAD}, equivalent SPAD capacitance C_{SPAD}).

III. RESULTS AND DISCUSSION

The internal capacitance $C_{SPAD} = 20.8$ aF and resistance $R_{SPAD} = 29.8$ kΩ are deduced from the *I-V* and *Q-V* characteristics (Figure 2), together with the breakdown voltage $V_B = 15.28$ V. These values of C_{SPAD} and R_{SPAD} are consistent with the limited cross section area of the simulated diode, i.e., smaller and higher, respectively, than the values commonly measured in real devices. Accordingly, for the quenching circuit, we have chosen values of R_Q and C_Q higher and smaller, respectively, than that used in real systems. Throughout the paper, a single value of C_Q of 0.1 fF has been used while values of R_Q ranging from 300 kΩ to

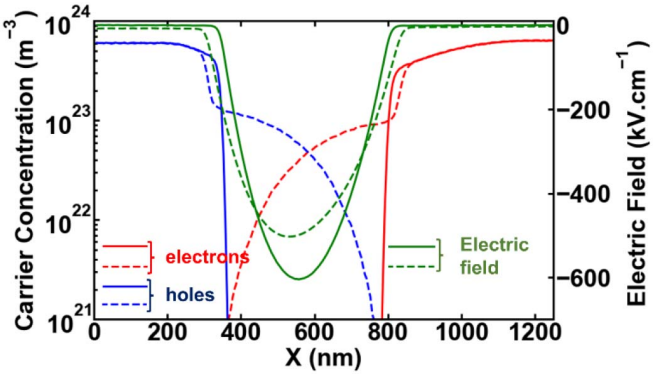

FIGURE 3. Carrier concentration for electrons (red lines) and holes (blue lines) and electric field profiles (green lines) for a constant voltage (Vbias = 18 V). These profiles are measured before (solid lines) and after breakdown (dotted lines).

1300 kΩ were considered. For $V_{bias} = 18$ V without quenching circuit ($R_Q = 0$ Ω, i.e., for a constant applied voltage $V_D = V_{bias}$) the depletion region of the junction extends from $X_{DEP1} = 360$ nm to $X_{DEP2} = 790$ nm with a maximum electric field of about 600 kV/cm (see Fig. 3). After the avalanche triggering, the current builds up in the device. The depletion region becomes wider and occupied by electrons and holes. Consistently, the electric field spans a wider zone and its maximum value is reduced down to 500 kV/cm (see Fig. 3).

In Fig. 4 are plotted (a) the number of impact ionization events, the time evolution of both (b) the current and (c) the voltage across the SPAD connected to a quenching circuit with $C_Q = 0.1$ fF and $R_Q = 500$ kΩ. The first e-h pair (resulting from photon absorption) is always generated at $t = 0$. Four different random choices of wave vectors of the initial e-h pair are presented. Green curves correspond to a successful quench, red curves show the case of successful quench, but after secondary avalanche breakdown onset, whereas blue and pink curves are typical examples of a non-successful quench.

The different behaviors can be separated in different phases marked by vertical lines in the figures. During the first phase, the first generated e-h pairs are accelerated by the electric field, which remains nearly frozen, and generates other e-h pairs, triggering an increase of current. During the second phase, after avalanche breakdown, through the effect of the quenching circuit, the strong increase of current leads to a decrease of voltage V_D and of electric field in the junction. This reduces the number of impact ionizations per free e-h pair.

During the third phase, the voltage across the SPAD becomes lower than the breakdown voltage, leading to a mean number of ionizations per generated carrier less than 1, which tends to break the avalanche process. Though it has been rarely reported, this undershoot voltage has been observed experimentally and analyzed by Inoue *et al.* [21]. We thus see a plateau in the cumulated number of impact ionization events and a strong current decrease. This current fall-off allows V_D to re-increase above V_B. We then enter the fourth phase that is critical for the success of the quench.

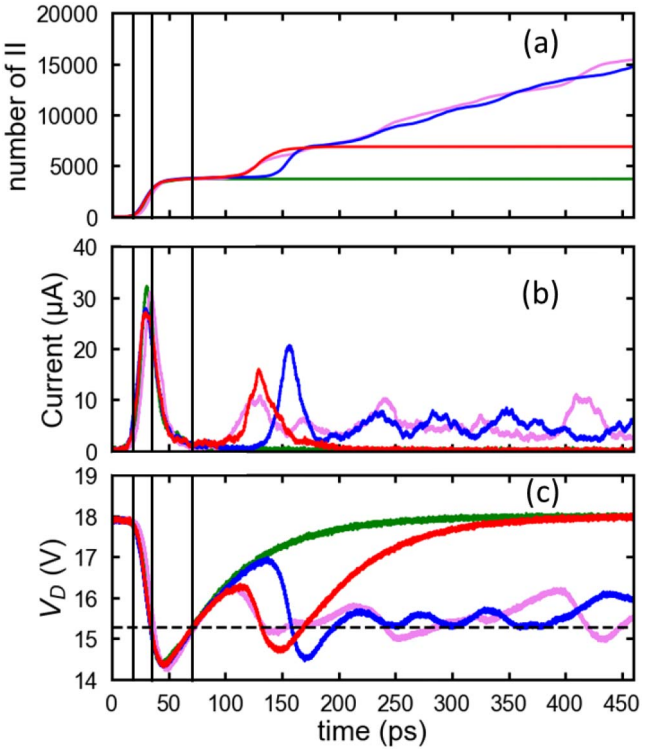

FIGURE 4. (a) Time evolution of the cumulated number of impact ionization events (II) for initial e-h pair generated at $t = 0$ s with a quenching circuit ($R_Q = 500$ kΩ, $C_Q = 0.1$ fF, $V_{bias} = 18$ V, $X_{GEN} = 500$ nm). Each color corresponds to a random set of wave vector coordinates of initial e-h pair. Vertical bars delimitate 4 different phases of operation, described in the text. (b) Corresponding time evolution of terminal current. (c) Corresponding time evolution of the SPAD voltage V_D.

If all e-h pairs have left the high-field region of SPAD the number of impact ionizations remains at the same level, the current vanishes, and V_D continues to increase up to V_{bias} and the quench is thus successful (green lines). In contrast, if some carriers remain in the high-field region during this fourth phase (when $V_D > V_{bias}$), a new breakdown may occur. In some cases, this secondary avalanche breakdown can eventually quench (red lines). It leads to an afterpulsing-like effect. However, this is not related to any trap assisted mechanism [22], but to a competing effect of deadtime and extinction time. When impact ionization events continue to occur, the current tends to oscillate around a finite value and the voltage across the SPAD cannot recover its initial value V_{bias} (blue and pink lines): the quench is not successful. It should be noted that when additional avalanches occur, the initial SPAD voltage may not be fully recovered within the typical RC circuit dead time. Thus, the effective dead time may increase statistically, without the presence of defects.

The simulation approach presented here is therefore very useful to explore the statistical features of the quench operation. To this goal, in addition to the avalanche breakdown probability, P_{BD}, previously discussed in other works [6], [7], we analyze the quenching probability, P_Q, as a function of the quenching resistance R_Q, together with the relevant characteristic times.

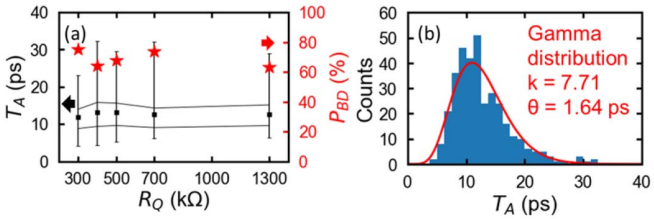

FIGURE 5. (a) Avalanche time T_A (black squares) and breakdown probability (red stars) versus quenching resistance R_Q for a constant value of $C_Q = 0.1$ fF. Black squares are mean values of T_A, while vertical bars indicate minimum and maximum values. Half of the values are in the closed area. (b) Avalanche time histogram for all values of R_Q.

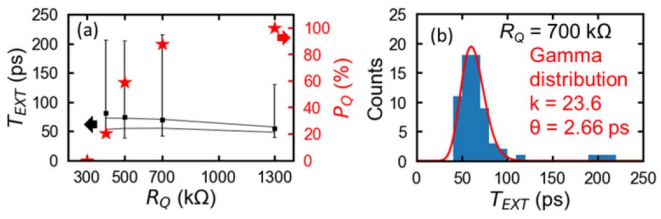

FIGURE 6. (a) Extinction time (black squares) and quenching probability (red stars) versus R_Q for a constant value of $C_Q = 0.1$ fF. Black squares are mean values, vertical bars indicate minimum and maximum values. Half of the values are in the closed area. (b) Extinction time histogram for $R_Q = 700$ kΩ and $C_Q = 0.1$ fF.

In some cases, although few e-h pairs have been generated, the cumulative number of ionization events quickly stops to increase instead of continuing its exponential increase. An avalanche breakdown can thus be characterized by two characteristic times. First, T_1 is the time interval between the creation of the initial e-h pair by photon absorption and the second e-h pair generation by impact ionization. For this specific SPAD with $V_{bias} = 18$ V and $X_{GEN} = 500$ nm, T_1 typically varies between 0.05 and 4.25 ps. Secondly, T_A, the time to avalanche, is the time when the number of impact ionizations is sufficient to self-maintain the exponential increase of the current. Here, T_A is defined as the time between the photon absorption and the time when the SPAD current (smoothed by rolling average over 2 ps) reaches a threshold value of 2 μA characterizing the breakdown regime. This time to avalanche may vary over a broad range in accordance with the statistical nature of the avalanche process and should be properly evaluated in order to accurately estimate the jitter.

Figure 5(a) shows the time to avalanche T_A and the breakdown probability as a function of R_Q varying from 300 kΩ to 1.3 MΩ (with $C_Q = 0.1$ fF). We observe that both quantities remain essentially independent of R_Q. This can be explained by the fact that they are measured just before the onset of avalanche breakdown, i.e., when the current is low and the quenching circuit has no influence on the internal SPAD state. The statistical distribution of the computed T_A is plotted in the histogram of Fig. 5(b) for 503 different simulations (346 breakdowns). This distribution can be well fitted by a gamma distribution with parameters k and θ of 7.71 and 1.64 ps, respectively. It confirms the large spreading of this quantity around the mean value of 12.6 ps with a standard deviation of 4.55 ps.

Figure 6(a) shows the quenching probability and the extinction time T_{EXT} as a function of R_Q. T_{EXT} is defined as the time between T_A and the last ionization event when the SPAD quenches. By considering a total time of 260 ps after photon absorption, i.e., about four times greater than the mean value of T_{EXT}, a quench is considered as successful if the last ionization event occurs before 230 ps. We observe that the extinction time T_{EXT} tends to reduce when increasing the resistance R_Q, while P_Q increases. Remarkably, this probability changes from 0% for $R_Q = 300$ kΩ to 100% for $R_Q = 1.3$ MΩ. This agrees with the analysis of [23] that explained why the quenching resistance must be high enough to obtain a successful quench. The histogram of the extinction time is plotted in Fig. 6(b) for $R_Q = 700$ kΩ in the cases of successful quenches (65 values have been used). Again, this distribution can be fitted with a gamma distribution, with parameters $k = 23.6$ and $\theta = 2.66$ ps. A large spreading of T_{EXT} is observed, as the standard deviation is 12.9 ps, for a mean value of 62.8 ps. It should be noted that the values of T_{EXT} greater than 150 ps have been excluded from the fitting procedure. They correspond to quenches after secondary avalanche and cannot be captured by the gamma distribution of single avalanche cases. As shown in Fig. 6(a), the quenching probability depends on the RC time constant of the moving node. Hence, a SPAD exhibiting a low quenching probability will not only increase its charge per pulse consumption, but also the recharge dead time. Experimentally, this may be tested by measuring pulse-width and inter-pulse time distributions [24].

IV. CONCLUSION

We have shown that, thanks to self-consistent 3-D MC simulation, together with a mixed-mode approach to include the passive quenching circuit, it is possible to capture the statistical properties of both avalanche and quenching stages of the SPAD electrical behavior. This study provides insights into SPAD operation in terms of avalanche and quenching probabilities as well as avalanche and extinction times. Such features are of high importance to optimally design this class of photodetectors.

REFERENCES

[1] E. Knill, R. Laflamme, and G. J. Milburn, "A scheme for efficient quantum computation with linear optics," *Nature*, vol. 409, pp. 46–52, Jan. 2001. [Online]. Available: https://doi.org/10.1038/35051009

[2] N. Gisin, G. Ribordy, W. Tittel, and H. Zbinden, "Quantum cryptography," *Rev. Modern Phys.*, vol. 74, no. 1, pp. 145–195, 2002. [Online]. Available: https://doi.org/10.1103/RevModPhys.74.145

[3] B. F. Aull *et al.*, "Three-dimensional imaging with arrays of Geiger-mode avalanche photodiodes," in *Proc. SPIE*, vol. 5353, 2004, p. 105. [Online]. Available: https://doi.org/10.1117/12.532723

[4] R. Cubeddu, D. Comelli, C. D'Andrea, P. Taroni, and G. Valentini, "Time-resolved fluorescence imaging in biology and medicine," *J. Phys. D Appl. Phys.*, vol. 35, no. 9, pp. R61–R76, 2002. [Online]. Available: https://doi.org/10.1088/0022-3727/35/9/201

[5] S. C. L. Tat Mun, C. H. Tan, Y. L. Goh, A. R. J. Marshall, and J. P. R. David, "Modeling of avalanche multiplication and excess noise factor in $In_{0.52}Al_{0.48}As$ avalanche photodiodes using a simple Monte Carlo model," *J. Appl. Phys.*, vol. 104, no. 1, 2008, Art. no. 013114. [Online]. Available: https://doi.org/10.1063/1.2952003

[6] J. D. Petticrew, S. J. Dimler, X. Zhou, A. P. Morrison, C. H. Tan, and J. S. Ng, "Avalanche breakdown timing statistics for silicon single photon avalanche diodes," *IEEE J. Sel. Topics Quantum Electron.*, vol. 24, no. 2, Art. no. 3801506, Mar./Apr. 2018. [Online]. Available: https://doi.org/10.1109/JSTQE.2017.2779834

[7] D. Dolgos, H. Meier, A. Schenk, and B. Witzigmann, "Full-band Monte Carlo simulation of high-energy carrier transport in single photon avalanche diodes: Computation of breakdown probability, time to avalanche breakdown, and jitter," *J. Appl. Phys.*, vol. 110, no. 10, 2012, Art. no. 084507. [Online]. Available: https://doi.org/10.1063/1.4717729

[8] R. Mita, G. Palumbo, and P. G. Fallica, "Accurate model for single-photon avalanche diodes," *IET Circuits Devices Sys.*, vol. 2, no. 2, pp. 207–212, 2008. [Online]. Available: https://doi.org/10.1049/iet-cds:20070180

[9] S. Cova, M. Ghioni, A. Lacaita, C. Samori, and F. Zappa, "Avalanche photodiodes and quenching circuits for single-photon detection," *Appl. Opt.*, vol. 35, no. 12, pp. 1956–1976, 1996. [Online]. Available: https://doi.org/10.1364/AO.35.001956

[10] F. Zappa, A.Tosi, A. DallaMora, and S.Tisa, "SPICE modeling of single photon avalanche diodes," *Sens. Actuators A Phys.*, vol. 153, no. 2, pp. 197–204, 2009. [Online]. Available: https://doi.org/10.1016/j.sna.2009.05.007

[11] Y. Oussaiti *et al.*, "Verilog-a model for avalanche dynamics and quenching in single-photon avalanche diodes," in *Proc. SISPAD*, 2020, pp. 145–148. [Online]. Available: https://doi.org/10.23919/SISPAD49475.2020.9241648

[12] D. A. Ramirez, M. M. Hayat, G. J. Rees, X. Jiang, and M. A. Itzler, "New perspective on passively quenched single photon avalanche diodes: Effect of feedback on impact ionization," *Opt. Exp.*, vol. 20, no. 2, pp. 1514–1522, 2012. [Online]. Available: https://doi.org/10.1364/OE.20.001512

[13] P. Dollfus, A. Bournel, S. Galdin-Retailleau, S. Barraud, and P. Hesto, "Effect of discrete impurities on electron transport in ultra-short MOSFET using 3D Monte Carlo simulation," *IEEE Trans. Electron Devices*, vol. 51, no. 5, pp. 749–756, May 2004. [Online]. Available: https://doi.org/10.1109/TED.2004.826844

[14] V. Aubry-Fortuna, P. Dollfus, and S. Galdin-Retailleau, "Electron effective mobility in strained-Si/$Si_{1-x}Ge_x$ MOS devices using Monte Carlo simulation," *Solid-State Electron.*, vol. 49, no. 8, pp. 1320–1329, 2005. [Online]. Available: https://doi.org/10.1016/j.sse.2005.06.013

[15] M. V. Fischetti and S. E. Laux, "Band structure, deformation potentials, and carrier mobility in strained Si, Ge, and SiGe alloys," *J. Appl. Phys.*, vol. 80, pp. 2234–2252, Apr. 1996. [Online]. Available: https://doi.org/10.1063/1.363052

[16] N. Goldsman, Y. J. Wu, and J. Frey, "Efficient calculation of ionization coefficients in silicon from the energy distribution function," *J. Appl. Phys.*, vol. 68, no. 3, pp. 1075–1081, 1990. [Online]. Available: https://doi.org/10.1063/1.346747

[17] Y. Kamakura *et al.*, "Impact ionization model for full band Monte Carlo simulation," *J. Appl. Phys.*, vol. 75, no. 7, pp. 3500–3506, 1994. [Online]. Available: https://doi.org/10.1063/1.356112

[18] R. Van Overstraeten and H. De Man, "Measurement of the ionization rates in diffused silicon p-n junctions," *Solid-State Electron.*, vol. 13, no. 5, pp. 583–608, 1970. [Online]. Available: https://doi.org/10.1016/0038-1101(70)90139-5

[19] W. Maes, K. De Meyer, and R. Van Overstraeten, "Impact ionization in silicon: A review and update," *Solid-State Electron.*, vol. 33, no. 6, pp. 705–718, 1990. [Online]. Available: https://doi.org/10.1016/0038-1101(90)90183-F

[20] S. Babiker, A. Asenov, N. Cameron, S. P. Beaumont, and J. R. Barker, "Complete Monte Carlo RF analysis of 'real' short-channel compound FET's," *IEEE Trans. Electron Devices*, vol. 45, no. 8, pp. 1644–1652, Aug. 1998. [Online]. Available: https://doi.org/10.1109/16.704358

[21] A. Inoue, T. Okino, S. Koyama, and Y. Hirose, "Modeling and analysis of capacitive relaxation quenching in a single photon avalanche diode (SPAD) applied to a CMOS image sensor," *Sensors*, vol. 20, no. 10, p. 3007, 2020. [Online]. Available: https://doi.org/10.3390/s20103007

[22] M. Hofbauer, B. Steindl, and H. Zimmermann, "Temperature dependence of dark count rate and after pulsing of a single-photon avalanche diode with an integrated active quenching circuit in 0.35μm CMOS," *J. Sens.*, vol. 2018, Jul. 2018, Art. no. 9585931. [Online]. Available: https://doi.org/10.1155/2018/9585931

[23] V. Savuskan, M. Javitt, G. Visokolov, I. Brouk, and Y. Nemirovsky, "Selecting single photon avalanche diode (SPAD) passive-quenching resistance: An approach," *IEEE Sensors J.*, vol. 13, no. 6, pp. 2322–2328, Jun. 2013. [Online]. Available: https://doi.org/10.1109/JSEN.2013.2253603

[24] D. Rideau *et al.*, "Single photon avalanche diode with monte carlo simulations: PDE, jitter and quench probability," in *Proc. Int. Conf. Simulation Semicond. Processes Devices (SISPAD),* 2021, pp. 293–296, , doi: 10.1109/SISPAD54002.2021.9592567.